

APPLICATION OF THE MULTILEVEL UV METHOD TO CALCULATE MICROWAVE ABSORPTION AND EMISSION OF OCEAN FOAM WITH KELVIN'S TETRAKAIDECAHEDRON STRUCTURE

Peng Xu,¹ Leung Tsang,^{1,2} and Dong Chen¹

¹ Department of Electronic Engineering
City University of Hong Kong
Hong Kong, P. R. China

² Electrical Engineering Department
University of Washington
Box 352500
Seattle, WA 98195-2500

Received 22 November 2004

ABSTRACT: Ocean foam is treated as densely packed air bubbles coated with thin walls of seawater. We choose a foam structure of the shapes of air bubbles based on Lord Kelvin's tetrakaidecahedron structure that has close to minimal contact surface area. We calculate the absorption coefficients from 1.5 to 36.5 GHz by using the multilevel UV method to accelerate the MoM solution. To illustrate the microwave emission, the brightness temperatures of a layer of foam above the ocean surface area calculated. © 2005 Wiley Periodicals, Inc. *Microwave Opt Technol Lett* 45: 445–450, 2005; Published online in Wiley InterScience (www.interscience.wiley.com). DOI 10.1002/mop.20849

Key words: volume scattering; microwave remote sensing; remote sensing of ocean; computational electromagnetics

1. INTRODUCTION

The foam on the ocean surface due to waves breaking plays an important role in the brightness temperatures of passive microwave remote-sensing of the ocean. To estimate the effect of the ocean foam on passive microwave remote-sensing measurements, various empirical microwave emissivity models have been used. Recently, a physically-based approach was proposed to model foam as air bubbles coated with seawater [1, 2]. The model treats foam as spherical air bubbles in a face-center-cubic (FCC) structure, and wave scattering and emission are solved using the quasi-crystalline approximation (QCA) in combination with dense-medium radiative-transfer (DMRT) theory [3].

Recently, a number of techniques such as the sparse-matrix canonical-grid method (SMCG) [4], the multilevel fast-multipole method (MLFMM) [5], the QR decomposition method [6], the multilevel UV method [7–9], the modified block-QR-factorization approach [10], and so forth, have been proposed to accelerate the impedance matrix-vector multiplication used in the iterative solution of the MoM matrix equation. The QR decomposition method is based on SVD, so it has thus far been demonstrated only for objects of moderate size in terms of wavelengths. The modified block-QR-factorization approach [10] has been applied to a single level and consists of the compression of dense MoM matrices based on low-rank singular-value decomposition with a single level, in which the rank is achieved using the dual-modified Gram–Schmidt (dual-MGS) method. The multilevel UV method has achieved $O(N \log N)$ based on the interpolation technique, with three steps: partitioning, searching the rank using SVD and coarse-coarse sampling, and building matrices U and V. Because the UV method operates on submatrices of the impedance matrix using tabulated values of the Green's values, it is hence applicable to all types of Green's functions. As it is applied independently to each level and each block, the procedure facilitates parallel imple-



Figure 1 Kelvin's Tetrakaidecahedron structure

mentation, although parallel implementation has not been implemented in this paper. The method can be applied to general impedance matrices constructed from more complicated Green's functions. For example, the multilevel UV method has also been applied to the volume-scattering problem of scatterers of moderate sizes with impedance matrices that consists of multiple partial waves [7].

In this paper, we study absorption and scattering using a realistic foam structure. The Kelvin-cell-shaped foam, with Tetrakaidecahedron structure, has close to minimal surface contact [11]. The computation is based on numerical solutions of scalar-wave equations. The solution of the MoM is accelerated by using the multilevel UV method.

In section 2, we describe the physical and geometric properties of the Kelvin's cell foam. Section 3 gives a description of the scalar-wave formulation used for scattering. Section 4 describes the multilevel UV method. In section 5, we describe the multilevel-partitioning process. In section 6, the numerical results are illustrated and discussed. In section 7, the simulated results of the absorption coefficients are incorporated into dense-media scalar-radiative transfer theory [12] in order to calculate the brightness temperatures of a layer of foam above the ocean surface.

2. FOAM DESCRIPTION

When air bubbles pack together to form foam, they are forced into polyhedral shapes as gravity extracts most of the liquid from their interstices. This is because surface energy has a great effect on liquid. Due to their lack of resistance to shear, bubbles take up shapes that minimize surface energy or its combination with other energy terms, such as gravitation [11]. Surface energy may be defined as the energy change of creating a unit area of a new surface or interface. So the geometry of interface in the foam is an important characteristic of its microstructure. In the single-bubble case, a spherical shape has the minimum surface area with a given volume. However, for the congregated bubbles, a conglomeration of spheres does not have the minimum contact area. Lord Kelvin studied the problem in 1887 and developed a structure named tetrakaidecahedron, or Kelvin's cell, as shown in Figure 1. The Kelvin's cell can be approximated by the truncated octahedron, and each is composed of six square faces and eight hexagonal faces with the same side length of a and wall thickness of t_j on each side of the j^{th} cell. The total wall thickness is then given by $t_i + t_j$, where i and j denote the two adjacent cells. The surface area and volume of each Kelvin's cell is $(6 + 12\sqrt{3})a^2$ and $8\sqrt{2}a^3$, respectively. The cells are packed in a body-centered-cubic (BCC) structure. In modeling foam, we let the interior of the cell be air while the wall is made of seawater. Using this structure, the fractional volume of seawater f_w is given by

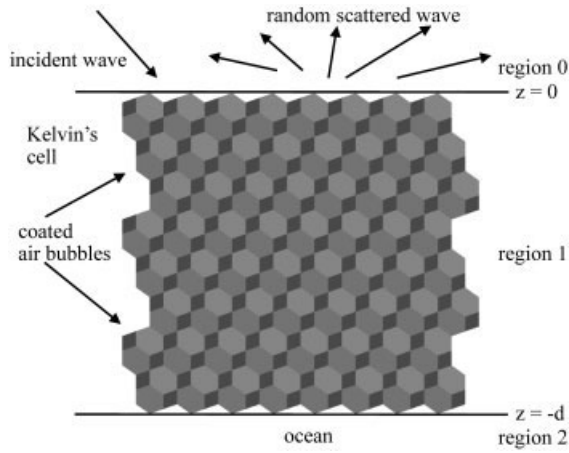


Figure 2 Geometrical configuration for thermal emission from foam-covered ocean (the foam layer is region 1 and is absorptive and scattering; region 2 is the ocean)

$$f_w = \int dt \frac{(6 + 12\sqrt{3})t}{8\sqrt{2}a} p(t) = \frac{(6 + 12\sqrt{3})\langle t \rangle}{8\sqrt{2}a}, \quad (1)$$

where $p(t)$ is the probability-density function of wall thickness t and the angular brackets represents averaging over t .

3. FORMULATION FOR SCALAR WAVE-SCATTERING

Consider a scalar plane-wave $\psi^{inc}(x, y, z)$ impinging on Kelvin's cells embedded in a background medium of air, as shown in Figure 2. Then the integral equation is given by

$$\psi(\bar{r}) = \psi^{inc}(\bar{r}) + k_0^2 \int_V g(\bar{r}, \bar{r}') (\epsilon_r(\bar{r}') - 1) \psi(\bar{r}') d\bar{r}', \quad (2)$$

where k_0 is the wavenumber in air, ϵ_r is relative permittivity of the cell wall, and $g(\bar{r}, \bar{r}') = \exp(ik_0|\bar{r} - \bar{r}'|)/4\pi|\bar{r} - \bar{r}'|$ is the Green's function in free space. The volume integral equation is discretized based on the discrete-dipole approximation (DDA) (as indicated on page 27 in [4]). We discretize every edge into n_0 segments. The total surfaces of each cell will be discretized into $30n_0^2$ hexahedrons. Every face is shared by two adjacent cells. We denote upper-half surfaces that include three square faces and four hexagonal faces, as shown in Figure 3, belonging to the cell. The other faces belong to its adjacent cells. Thus, each cell has $M = 15n_0^2$ unknowns and these unknowns are no longer shared by other cells. The thickness of the hexahedrons is then $(t_j + t_i)$, which are different in different faces. There are two kinds of hexahedrons: one is a square from the square faces; the other is a diamond from the hexagonal faces, as shown in Figure 3. Then, the integral equation can be transformed as follows:

$$\psi_m = \psi_m^{inc} + k_0^2 (\epsilon_r - 1) \sum_{\substack{n=1 \\ n \neq m}}^N g(\bar{r}_m, \bar{r}_n) \psi_n \Delta V_n + \psi_{self} \quad (3)$$

where the self term $\psi_{self} = k_0^2 (\epsilon_r - 1) \int_{\Delta V_m} g(\bar{r}_m, \bar{r}') \psi_m d\bar{r}'$ can be calculated using the Duffy's transform method [13]. Equation (3) is written in the form of a matrix equation as

$$\bar{\bar{Z}}\bar{\bar{y}} = \bar{\bar{b}}, \quad (4)$$

$$\bar{\bar{\Delta}}\bar{\bar{x}} = \bar{\bar{y}}, \quad (5)$$

where

$$Z_{mn} = \begin{cases} k_0^2(1 - \epsilon_r) g(\bar{r}_m, \bar{r}_n) & n \neq m \\ \left[1 - k_0^2(\epsilon_r - 1) \int_{\Delta V_m} g(\bar{r}_m, \bar{r}') d\bar{r}' \right] / \Delta V_m & n = m \end{cases} \quad (6)$$

$$b_m = \psi_m^{inc}, \quad (7)$$

$$\Delta_{mn} = \begin{cases} 0 & n \neq m \\ \Delta V_m & n = m \end{cases} \quad (8)$$

$$x_n = \psi_n = y_n / \Delta V_n. \quad (9)$$

By using Eqs. (4) and (5), we solve directly not $\bar{\bar{x}}$ but $\bar{\bar{y}}$, such that there are many of the same blocks in impedance matrix $\bar{\bar{Z}}$ and much memory will be saved.

After solving the matrix equations, the absorption coefficient κ_{abs} can be calculated as follows [2]:

$$\kappa_{abs} = \frac{P_{abs}}{\frac{1}{2\eta} |\psi^{inc}|^2 V} = \frac{\omega \epsilon'' \eta}{|\psi^{inc}|^2 V} \sum_{n=1}^N |\psi_n|^2 \Delta V_n, \quad (10)$$

where P_{abs} is the power absorbed by foam, ω is the angular frequency of the exciting field, ϵ'' is the imaginary part of the permittivity of cell wall, η is the free-space wave impedance, and V is the total volume of the foam in the simulations, including the air space.

4. THE MULTILEVEL UV METHOD

In solving the matrix equation, we apply the multilevel UV method to accelerate the iterative solver. For a specific scattering problem with a given geometry, the scattering structure is partitioned into multilevel blocks. Consider a block \bar{A} of dimensions $N_0 \times N_0$, which represents the interactions of a transmitting group and a nonneighbor receiving group. We can use the SVD to determine the rank. Let σ_1 be the largest singular value and the singular values be arranged in decreasing magnitude. Given a threshold ϵ , the rank r is such that

$$\left| \frac{\sigma_{r+1}}{\sigma_1} \right| \leq \epsilon.$$

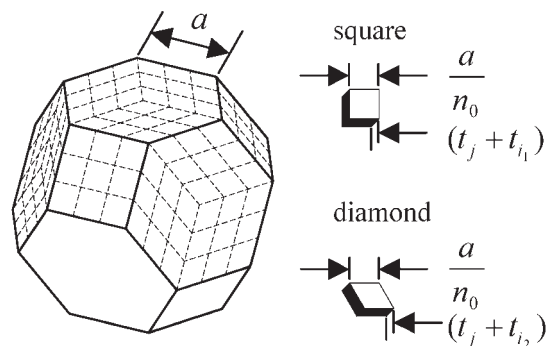


Figure 3 Discretization of Kelvin's cell

If the size of the block \bar{A} becomes larger, it would consume CPU memory intensively. However, generally the rank is much smaller than the size of the block. Thus, we can use coarse-coarse sampling for searching the rank. Namely, we uniformly pick the number of points in the transmitting group and a set of points in the receiving group, and form a new matrix of dimensions that are slightly larger than the rank, and we find the rank via the new matrix to be roughly same as that via the block \bar{A} . This means we have a prior knowledge of roughly what is the rank, based on the numerical experiments carried out. As an exact rank is not required, in coarse sampling we can pick the number of points to be several times larger than the rank.

By looking up its rank r with the SVD and fast coarse-coarse sampling, the block \bar{A} is expressed as

$$\bar{A}_{N_0 \times N_0} = \bar{U}_{N_0 \times r} \bar{V}_{r \times N_0}, \quad (11)$$

where $\bar{V}_{r \times N_0} = (\bar{U}_{r \times r})^{-1} \bar{R}_{r \times N_0}$ is calculated by LU decomposition using Crout's method with partial pivoting instead of an inversion of \bar{U} . The columns of \bar{U} are r columns of \bar{A} with uniform distribution, the rows of \bar{R} are r rows of \bar{A} with uniform distribution, and the rows of \bar{U} are r rows of \bar{U} with uniform distribution [7–9].

Generally, the rank of the block is much less than its dimension, so that in an iterative solution to the matrix equation, using matrices U and V instead of the block matrix to multiply with a vector, the computational time and memory requirement can be decreased from $O(N_0^2)$ to $O(2rN_0)$.

5. IMPLEMENTATION OF METHODOLOGY

The total number of coated Kelvin's cells, which are arranged in a BCC structure, is $8 \times 8 \times 8$ in three orthogonal directions. We label every cell, as shown in Figure 4. The 64 subgroups of 1st-level, which are marked as $1_1, 2_1, \dots, 8_1; 65_1, 66_1, \dots, 72_1; 129_1, 130_1, \dots, 136_1; \text{ and } 449_1, 450_1, \dots, 456_1$ are, namely, the layer shown in Figure 2. We define index coordinates to identify the cells. For example, the group 1_1 has index coordinate $(1_1, 1_1, 1_1)$, 80_1 has $(8_1, 2_1, 2_1)$, 19_2 has $(3_2, 1_2, 2_2)$, and so on. It is more convenient to use index coordinates than to use actual coordinates directly. Every subgroup of 1st level is a Kelvin's cell with M elements, for example, in subgroup 1_1 , there are elements of $1, 2, \dots, M$; in subgroup 2_1 , there are elements of $M + 1, M + 2, \dots, 2M$; and so on. The total number of unknowns is given by

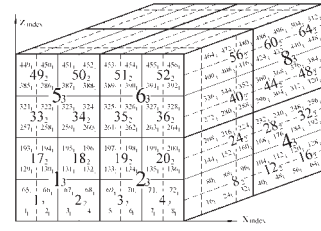


Figure 4 The multilevel partitioning process

$$N = M2^{3(p+1)}, \quad (12)$$

where p is the number of total level. For this case, $p = 2$. To facilitate understanding of the multilevel partitioning process, Figure 4 also shows the level-2 group marked as $1_2, 2_2, \dots, 64_2$, and the level-3 groups marked as $1_3, 2_3, \dots, 8_3$. Each of the level-2 groups has eight level-1 groups and each of the level-3 groups has eight level-2 groups. For example, the group 3_2 has eight groups of $5_1, 6_1, 13_1, 14_1, 69_1, 70_1, 77_1$, and 78_1 and the group 2_3 has eight groups of $3_2, 4_2, 7_2, 8_2, 19_2, 20_2, 23_2$, and 24_2 .

Now we decompose the full impedance matrix \bar{Z} as the summation of $(p + 1)$ sparse matrices as follows:

$$\bar{Z} = \bar{Z}^{(0)} + \bar{Z}^{(1)} + \bar{Z}^{(2)} + \dots + \bar{Z}^{(p)}. \quad (13)$$

Matrix $\bar{Z}^{(0)}$ includes all the interactions among neighboring groups (including self group) at the first level. Matrix $\bar{Z}^{(1)}$ includes all the interactions among neighboring groups at the 2nd level, excluding those that have been included by $\bar{Z}^{(0)}$. Similarly, matrix $\bar{Z}^{(i)}$ includes all the interactions among neighboring groups at the $(i + 1)$ th level, excluding those that have been included by $\bar{Z}^{(i-1)}$.

We use m_i to represent the group m of the level i . Then matrix $\bar{Z}_{m_i n_i}$ represents the interactions between the receiving group m and transmitting group n of the i th level. Since the i th-level group has eight $(i - 1)$ th-level groups, we obtain $\bar{Z}_{m_i n_i}$ with $M \times M$ dimensions and $\bar{Z}_{m_2 n_2}$ with $8M \times 8M$ dimensions. For example,

$$\bar{Z}_{3_2 1_2} = \begin{bmatrix} \bar{Z}_{5_1 1_2 9_1} & \bar{Z}_{5_1 1_3 0_1} & \bar{Z}_{5_1 1_3 7_1} & \bar{Z}_{5_1 1_3 8_1} & \bar{Z}_{5_1 1_9 3_1} & \bar{Z}_{5_1 1_9 4_1} & \bar{Z}_{5_1 2_0 1_1} & \bar{Z}_{5_1 2_0 2_1} \\ \bar{Z}_{6_1 1_2 9_1} & \bar{Z}_{6_1 1_3 0_1} & \bar{Z}_{6_1 1_3 7_1} & \bar{Z}_{6_1 1_3 8_1} & \bar{Z}_{6_1 1_9 3_1} & \bar{Z}_{6_1 1_9 4_1} & \bar{Z}_{6_1 2_0 1_1} & \bar{Z}_{6_1 2_0 2_1} \\ \bar{Z}_{1_3 1_2 9_1} & \bar{Z}_{1_3 1_3 0_1} & \bar{Z}_{1_3 1_3 7_1} & \bar{Z}_{1_3 1_3 8_1} & \bar{Z}_{1_3 1_9 3_1} & \bar{Z}_{1_3 1_9 4_1} & \bar{Z}_{1_3 2_0 1_1} & \bar{Z}_{1_3 2_0 2_1} \\ \bar{Z}_{1_4 1_2 9_1} & \bar{Z}_{1_4 1_3 0_1} & \bar{Z}_{1_4 1_3 7_1} & \bar{Z}_{1_4 1_3 8_1} & \bar{Z}_{1_4 1_9 3_1} & \bar{Z}_{1_4 1_9 4_1} & \bar{Z}_{1_4 2_0 1_1} & \bar{Z}_{1_4 2_0 2_1} \\ \bar{Z}_{6_9 1_2 9_1} & \bar{Z}_{6_9 1_3 0_1} & \bar{Z}_{6_9 1_3 7_1} & \bar{Z}_{6_9 1_3 8_1} & \bar{Z}_{6_9 1_9 3_1} & \bar{Z}_{6_9 1_9 4_1} & \bar{Z}_{6_9 2_0 1_1} & \bar{Z}_{6_9 2_0 2_1} \\ \bar{Z}_{7_0 1_2 9_1} & \bar{Z}_{7_0 1_3 0_1} & \bar{Z}_{7_0 1_3 7_1} & \bar{Z}_{7_0 1_3 8_1} & \bar{Z}_{7_0 1_9 3_1} & \bar{Z}_{7_0 1_9 4_1} & \bar{Z}_{7_0 2_0 1_1} & \bar{Z}_{7_0 2_0 2_1} \\ \bar{Z}_{7_7 1_2 9_1} & \bar{Z}_{7_7 1_3 0_1} & \bar{Z}_{7_7 1_3 7_1} & \bar{Z}_{7_7 1_3 8_1} & \bar{Z}_{7_7 1_9 3_1} & \bar{Z}_{7_7 1_9 4_1} & \bar{Z}_{7_7 2_0 1_1} & \bar{Z}_{7_7 2_0 2_1} \\ \bar{Z}_{7_8 1_2 9_1} & \bar{Z}_{7_8 1_3 0_1} & \bar{Z}_{7_8 1_3 7_1} & \bar{Z}_{7_8 1_3 8_1} & \bar{Z}_{7_8 1_9 3_1} & \bar{Z}_{7_8 1_9 4_1} & \bar{Z}_{7_8 2_0 1_1} & \bar{Z}_{7_8 2_0 2_1} \end{bmatrix}. \quad (14)$$

5.1. The Blocks in $\bar{Z}^{(0)}$

In $\bar{Z}^{(0)}$, there are two kinds of blocks: diagonal blocks (that is, self interactions) and nondiagonal blocks (that is, interactions between neighboring 1st-level groups. Because all cells have the same side length a , diagonal blocks such as $\bar{Z}_{1_1 1_1}$ and $\bar{Z}_{m_1 m_1}$ are all the same, except for their diagonal elements; therefore, we calculate only one

diagonal block and N diagonal elements. In the numerical solution of the matrix equation, the inversion of diagonal blocks is used as a preconditioner. We have interactions of level-1 groups with their nearest neighbors. Each group has $3^3 - 1 = 26$ nearest neighbors, except that face level-1 groups such as 131_1 have only 17 neighbors, edge level-1 groups such as 4_1 have only 11 neighbors, and

corner level-1 groups such as 8_1 have only seven neighbors. For example, 75_1 has neighbors of

$$\begin{array}{cccccc} 18_1 & 19_1 & 20_1 & 82_1 & 83_1 & 84_1 \\ 10_1 & 11_1 & 12_1 & 74_1 & & 76_1, \\ 2_1 & 3_1 & 4_1 & 66_1 & 67_1 & 68_1 \end{array}$$

and

$$\begin{array}{ccc} 146_1 & 147_1 & 148_1 \\ 138_1 & 139_1 & 140_1, \\ 130_1 & 131_1 & 132_1 \end{array}$$

Thus, the 26 impedance blocks of $\bar{Z}_{2,75_1}, \bar{Z}_{3,75_1}, \dots, \bar{Z}_{148,75_1}$, each with $M \times M$ dimensions, are in $\bar{Z}^{(0)}$. We use the index coordinates and the distance between the index coordinates of two level-1 groups to judge whether the two groups are neighbors. Because these blocks have neighbor interactions at the 1st level, they cannot be decomposed by the UV method; however, they can be decomposed directly by the SVD-based QR method due to their small dimensions. In addition, we change matrix equation into the form of Eq. (4), so that most nondiagonal blocks in $\bar{Z}^{(0)}$ are same, and only matrices U and V of the different blocks are recorded; hence, memory is saved.

5.2. The Blocks in $\bar{Z}^{(1)}$

In $\bar{Z}^{(1)}$, we select the interactions between level-2 groups and their nearest neighbors and exclude those that have been included in $\bar{Z}^{(0)}$. For example, for 131_1 in 18_2 , we firstly search the neighbors of 18_2 using the index coordinate and index distance at the 2nd level. We then obtain its neighbors as follows:

$$\begin{array}{cccccc} 5_2 & 6_2 & 7_2 & 21_2 & 22_2 & 23_2 \\ 1_2 & 2_2 & 3_2 & 17_2 & & 19_2, \end{array}$$

and

$$\begin{array}{ccc} 37_2 & 38_2 & 39_2 \\ 33_2 & 34_2 & 35_2, \end{array}$$

Secondly, every 1st-level group in the 2nd-level neighbor groups is selected to interact with 131_1 , except for blocks that have been included by $\bar{Z}^{(0)}$. For instance, we select $1_1, 2_1, 9_1, 10_1, 65_1, 66_1, 73_1$, and 74_1 of 1_2 by using the index coordinate and index distance at the 1st-level, and exclude 66_1 and 74_1 of 1_2 , which are neighbors of 131_1 in $\bar{Z}^{(0)}$. Then $\bar{Z}^{(1)}$ includes blocks of $\bar{Z}_{1,131_1}, \bar{Z}_{2,131_1}, \bar{Z}_{9,131_1}, \bar{Z}_{10,131_1}, \bar{Z}_{65,131_1}$, and $\bar{Z}_{73,131_1}$ with dimensions $M \times M$. Now we select 1st-level groups of 2_2 again to interact with 131_1 , until the 1st-level groups of all the 2nd-level neighbors are interacting with 131_1 . After these processes, we reprocess with 132_1 in 18_2 , as with 131_1 , until all 1st-level groups in 18_2 interact with their neighbors, and so on. These blocks in $\bar{Z}^{(1)}$ are decomposed into matrices U and V using the UV method. Similarly, as many blocks are the same, much memory is saved.

5.3. The Blocks in $\bar{Z}^{(2)}$

In $\bar{Z}^{(2)}$, we select the interactions between level-3 groups and their nearest neighbors and exclude those that have been included by $\bar{Z}^{(1)}$. For example, for 18_2 in 1_3 , we find that 1_3 has neighbors of $2_3, 3_3, \dots, 8_3$. Choosing 2_3 as an example, we select $4_2, 8_2, 20_2$, and 24_2 of 2_3 to interact 18_2 , and exclude $3_2, 7_2, 19_2$, and 23_2 of 2_3 because they are neighbors of 18_2 in $\bar{Z}^{(1)}$. Thus, $\bar{Z}^{(2)}$ includes blocks of $\bar{Z}_{4,18_2}, \bar{Z}_{8,18_2}, \bar{Z}_{20,18_2}$, and $\bar{Z}_{24,18_2}$ with dimensions

TABLE 1 Permittivity as a Function of Frequency

Frequency [GHz]	ϵ_r
1.5	74.714 + $i53.705$
5.0	66.499 + $i37.428$
10.8	49.149 + $i40.105$
18.0	29.090 + $i37.362$
36.5	13.448 + $i24.784$

$8M \times 8M$. These blocks are decomposed into matrices U and V using the UV method.

Higher-level blocks can be handled in the same manner as those in $\bar{Z}^{(2)}$. For all blocks, we must also record their receiving and transmitting indices. UV decomposition needs to be done only once and does not need to be repeated for each iteration. The CPU of the UV decomposition is included as preprocessing.

6. NUMERICAL RESULTS AND DISCUSSION

In the following, we illustrate the numerical results of the absorption coefficient based upon assembling Kelvin's cell in a BCC structure. We summarize the foam parameters as follows: a is the side length of all cells, t_j is the wall thickness of the j^{th} cell, $\langle t \rangle$ is the average wall thickness of cells, $p(t)$ is the probability-density function of wall thickness, f_w is the fractional volume of seawater in foam, ϵ_r is the complex permittivity of seawater, N_c is the number of cells, and V is the total sample volume.

Note that the permittivity of seawater ϵ_r is a function of the frequency and other physical parameters, such as the temperature and salinity. In our simulation, the permittivities of seawater at five frequencies are listed in Table 1, which are given by the Debye expression [14]:

$$\epsilon_r = \epsilon_\infty + \frac{\epsilon_1 - \epsilon_\infty}{1 - i\omega\tau} + \frac{i\sigma}{\omega\epsilon_0}, \quad (15)$$

where ϵ_0 is the permittivity of free space, $\epsilon_\infty = 4.9$, and τ, σ are functions of the seawater temperature ($^\circ\text{C}$) and the salinity (g salt/kg water), in which we choose temperature and the salinity of seawater to be 10°C and 35 g salt/kg water, respectively. The five frequencies are the common channels in satellite passive-microwave remote sensing, for example, the AQUA and WINDSAT satellites. The total number of coated Kelvin's cells is $N_c = 8 \times 8 \times 8 = 2^{3(p+1)}$ in three orthogonal directions. The total number of unknowns is given by

$$N = MN_c = 15n_0^2 2^{3(p+1)} = 69120. \quad (16)$$

In the simulations, $a = 0.672$ mm and $n_0 = 3$. We let f_w be 0.2%, 1%, 3%, and 5%. From Eq. (1) we can obtain the average wall thickness $\langle t \rangle$ at different f_w . In addition, let $p(t)$ be the Rayleigh distribution:

$$p(t) = \frac{t}{\sigma^2} \exp\left(-\frac{t^2}{2\sigma^2}\right), \quad (17)$$

where $\sigma = \sqrt{2/\pi} \langle t \rangle$, then $t_j, j = 1, 2, \dots, N_c$ with the Rayleigh distribution generated by the cumulative distribution function:

$$F(t) = 1 - \exp\left(-\frac{t^2}{2\sigma^2}\right), \quad (18)$$

TABLE 2 CPU Time for the UV-CG Method with Frequency of 36.5 GHz, $a = 0.672$ mm and $N = 69120$ Unknowns

f_w [%]	Preprocessing [sec]	Time Per Iteration [sec]	Number of Iterations	Total Time [sec]
5.0	566	76.6	16	1.792
0.2	565	76.3	3	794

where the $F(t)$ values are generated with uniformly distributed N_c random numbers between 0 and 1. The total volume $V = 8\sqrt{2} a^3 N_c$.

6.1. CPU Time for the UV Method

In Table 2, we list the CPU at 36.5 GHz, based on the UV method for the simulations illustrated using a single 2.66-GHz processor. The convergent condition for the iterative approach is set at $2.5e-3$. The preprocessing time of the UV method is the time used to search the rank and to construct the U and V matrices, including the nondiagonal block at the 0th level. For each case, CPU time of less than 77 sec per iteration, total CPU time less than 1,792 sec, and memory of less than 700 MB with 69,120 unknowns are required. We also show the number of iterations. The number of iterations at lower f_w is smaller than that at higher f_w . At other frequencies, the CPUs are all less than that at 36.5 GHz, and the memory requirements are less than 700 MB for all cases.

6.2. The Absorption Coefficient

In Table 3, the calculated absorption coefficients, in which the absorption coefficient is slightly different for different realizations, are tabulated. In Figure 5, we plot the absorption coefficients as a function of the frequencies at different f_w . It is shown that the absorption rate increases with the increase of frequency at lower f_w . However, the trend is reversed at higher f_w . These results show that the absorption coefficient depends strongly on frequency and fractional volume. At lower f_w , the wave at both high and low frequencies can penetrate into the cell walls. Then the absorption coefficient at high frequency is larger than that at low frequency. At higher f_w , it becomes difficult to penetrate the cell walls at high frequency. Thus, the foam at high frequency has smaller absorption coefficient.

We next plot the absorption coefficients as a function of f_w at different frequencies, as shown in Figure 6. The absorption coefficient is shown to increase with an increase of f_w at low frequency. With the increase of frequency, the absorption coefficient shows saturation with the increase of f_w .

7. NUMERICAL SIMULATIONS OF BRIGHTNESS TEMPERATURE

We use the simulated results of the absorption coefficient with radiative-transfer theory [12] in order to compute the brightness temperatures for horizontal polarization and vertical polarization at 1.5, 5.0, and 10.8 GHz. At these frequencies, the albedos are small and only the absorption effects are important. The permittivities of

TABLE 3 Numerical Result of Absorption Coefficient (cm^{-1})

f [GHz] \ f_w [%]	0.2	1.0	3.0	5.0
1.5	0.038	0.175	0.622	1.105
5.0	0.090	0.487	1.493	2.019
10.8	0.170	0.675	1.351	1.640
18.0	0.275	0.923	1.565	1.721
36.5	0.328	0.999	1.481	1.524

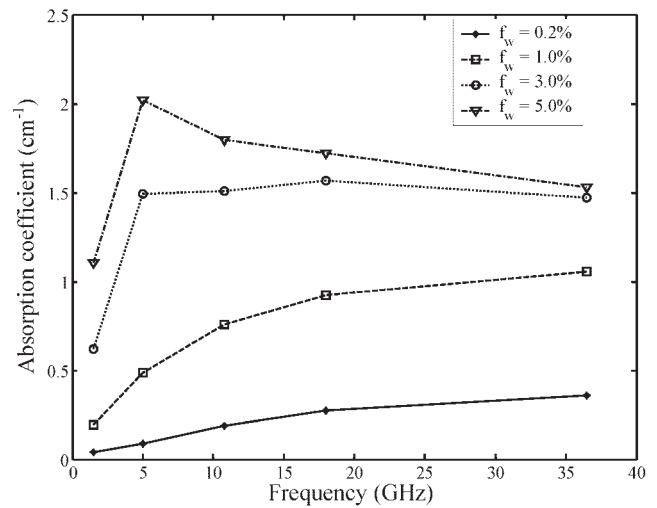


Figure 5 Absorption coefficient as a function of frequency

seawater are shown in Table 1 with a seawater temperature of 10°C. The side length of the foam is 0.672 mm and $f_w = 1.0\%$. The absorption rates are shown in the third column of Table 3. The thickness of the foam layer is 1.09 cm. In Figure 7, the brightness temperatures for the vertical and horizontal polarizations are plotted as a function of frequency at an observation angle of 55°. It is shown that the brightness temperatures increase with the increase of frequency.

8. CONCLUSION

We have applied the multilevel UV method to accelerate the MoM solution and analyze the absorption coefficient of Kelvin's foam on a surface of seawater. The numerical simulations have shown the dependence of absorption on frequency and on the microstructure properties such as size and surface-to-volume ration. Presently, we are extending the model to vector electromagnetic waves using Maxwell's equations.

ACKNOWLEDGMENTS

This work was supported by the Office of Naval Research, Hong Kong RGC Central Allocation grant no. 8730017, and Hong Kong RGC CERG grant no. 9040935.

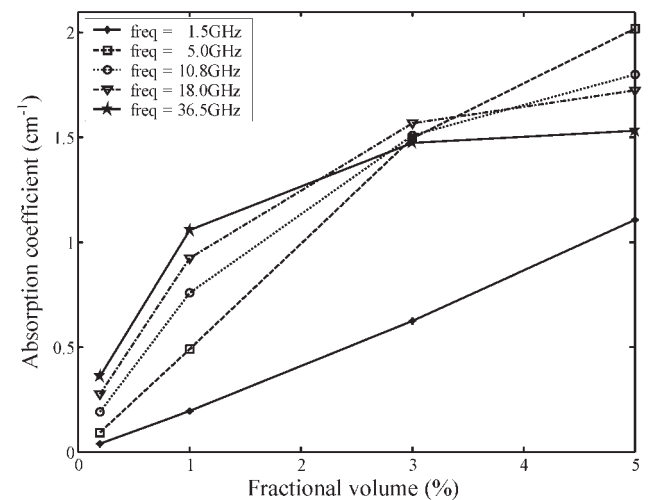


Figure 6 Absorption coefficient as a function of the fractional volume of seawater

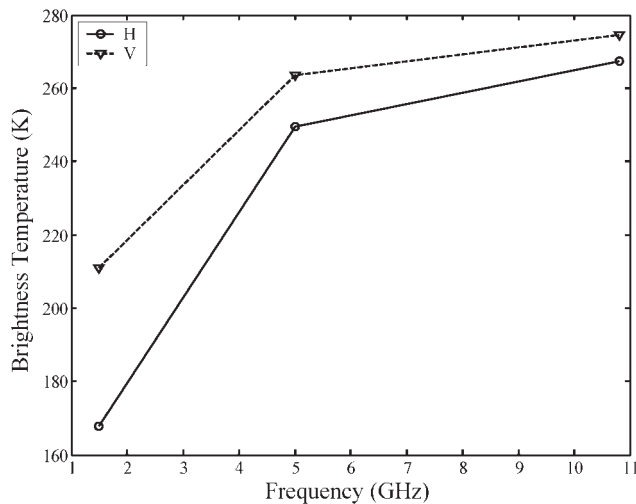


Figure 7 Brightness temperature as a function of frequency at 55° observation angle (the temperature of seawater is 10°C; the side length of Kelvin's cell is 0.672 mm; f_w is 1.0%)

REFERENCES

1. J. Guo, L. Tsang, W. Asher, K.-H. Ding, and C.-T. Chen, Application of dense media radiative transfer theory for passive microwave remote sensing of foam covered ocean, *IEEE Trans Geosci Remote Sensing* 39 (2001), 1019–1027.
2. D. Chen, L. Tsang, L. Zhou, S.C. Reising, W. Asher, L.A. Rose, K.H. Ding, and C.-T. Chen, Microwave emission and scattering of foam based on Monte Carlo simulations of dense media, *IEEE Trans Geosci Remote Sensing* 41 (2003), 782–790.
3. L. Tsang and J.A. Kong, Scattering of electromagnetic waves, *Adv Topics 3*, John Wiley, New York (2001), p. 300.
4. L. Tsang, J.A. Kong, K.H. Ding, and C.O. Ao, Scattering of electromagnetic waves, *Numer Simulations 2* (2001), 179–190.
5. V. Jandhyala, B. Shanker, E. Michielssen, and W.C. Chew, A fast algorithm for the analysis of scattering by dielectric rough surfaces, *J Opt Soc Am A* 15 (1998), 1877–1885.
6. S. Kapur and D.E. Long, IES³: A fast integral equation solver for efficient 3-dimensional extraction, *Proc 37th Int Conf Computer Aided Design*, 1997, pp. 448–455.
7. L. Tsang and Q. Li, Wave scattering with UV multilevel partitioning method for volume scattering by discrete scatterers, *Microwave Opt Technol Lett* 41 (2004), 354–361.
8. L. Tsang, D. Chen, P. Xu, Q. Li, and V. Jandhyala, Wave scattering with the UV multilevel partitioning method: 1. Two-dimensional problem of perfect electric conductor surface scattering, *Radio Sci* 39 (2004).
9. L. Tsang, Q. Li, P. Xu, D. Chen, and V. Jandhyala, Wave scattering with UV multi-level partitioning method 2: three-dimensional problem of nonpenetrable surface scattering, *Radio Sci* 39 (2004).
10. R.J. Burkholder and J.F. Lee, Fast dual-MGS block-factorization algorithm for dense MoM matrices, *IEEE Trans Antennas Propagat* 52 (2004), 1693–1699.
11. D. Weaire and S. Hutzler, *The physics of foams*, Clarendon Press, Oxford, 1999, pp. 152–158.
12. L. Tsang, J.A. Kong, and K.H. Ding, Scattering of electromagnetic waves. *Theories and Applic 1*, John Wiley, New York (2000), 260–268.
13. M.G. Duffy, Quadrature over a pyramid or cube of integrands with a singularity at a vertex, *SIAM J Numer Anal* 19 (1982), 1260–1262.
14. L.A. Klein and C.T. Swift, An improved model for the dielectric constant of sea water at microwave frequencies, *IEEE Trans Antennas Propagat AP-25* (1977), 104–111.

© 2005 Wiley Periodicals, Inc.

EVIDENCE OF BIREFRINGENCE AND ANOMALOUS ELECTROMAGNETIC-PULSE PROPAGATION IN AN ORGANIC LIGHT-EMITTING DIODE

Sheng-Chieh Tai,¹ Jyh-Long Chern,¹ Yueh-Chuan Huang,² Mei-Rung Tseng,² and Hsien-Kuang Lin²

¹ Department of Photonics
Institute of Electro-Optical Engineering, Display Institute
Microelectronics and Information System Research Center
National Chiao Tung University
Hsinchu 300, Taiwan
² Material Research Laboratory
Industrial Technology Research Laboratory
Hsinchu, Taiwan

Received 3 December 2004

ABSTRACT: High-speed electromagnetic characteristics of an organic light-emitting diode (OLED) are explored in this paper. When a high-frequency (~14 GHz) microwave pulse is injected into an OLED, the pulse is split into two peaks: one peak is delayed by 1.725 ns and another one is advanced by 0.183 ns, which also suggests the existence of an extremely low-speed group velocity. The effective thickness of the OLED sample is ~355.8 nm and, as a result, the effective index of refraction is ~10⁷ when the splitting phenomenon occurs. © 2005 Wiley Periodicals, Inc. *Microwave Opt Technol Lett* 45: 450–452, 2005; Published online in Wiley InterScience (www.interscience.wiley.com). DOI 10.1002/mop.20850

Key words: organic light-emitting diode; superluminal effect; electro-magnetic-pulse propagation

1. INTRODUCTION

Electromagnetic-pulse propagation has been a longstanding issue, ever since the founding of electromagnetic theory by Maxwell [1], and efforts to revisit this classical topic are readily found in the literature. It also has provided a variety of novel applications such as fiber communication and soliton communication [2]. On the other hand, there is an intriguing topic concerning the fundamental aspect of electromagnetic theory, that is, the propagation limit set by the velocity of light. It is known that the velocity of an electromagnetic pulse passing through a normal dispersive medium is well characterized by group velocity. According to classical theory [1], the group velocity of a pulse in linear dispersion and a nonabsorbing medium is described as

$$v_g = \frac{d\omega}{dk} = \frac{c}{n(\omega) + \omega(dn/d\omega)}, \quad (1)$$

where ω and k are the angular frequency and wave vector of the electromagnetic wave, respectively, and c is the velocity of light in a vacuum. Typically, v_g is less than c . But, for an anomalous dispersion, $dn/d\omega < 0$, which leads to v_g being larger than c . This violates the theory of relativity, which states that no velocity can be larger than c . Actually, in this case the group velocity lost its meaning as a signal velocity [3]. Indeed, contrary to common group velocity, Brillouin introduced the energy velocity v_E , which is more meaningful [3]. The true energy velocity can be defined as the rate of energy flow divided by the stored energy density of the electromagnetic wave, as correctly derived by Loudon [4], even though an anomalous dispersion leads the pulse to seemingly advance. This phenomenon of pulse advance is referred to as the “superluminal effect.” Given the current interest, one can find the superluminal effect in the literature, with regard to passive absorp-